*36th EPS Conference on Plasma Phys. Sofia, June 29 - July 3, 2009 ECA Vol.**33E**, P-4.121 (2009)*

Finite Larmor radius effects on test particle transport in drift wave-zonal flow turbulence

J M Dewhurst[1], B Hnat[1] and R O Dendy[2,1]

[1]*Centre for Fusion, Space and Astrophysics, University of Warwick, Coventry CV4 7AL, U.K.*
[2]*Euratom/UKAEA Fusion Association, Culham Science Centre, Oxfordshire OX14 3DB, U.K.*

Introduction. It is widely recognised that zonal flows play an important role in the self-regulation of drift wave turbulence. The response of particles to turbulent fields can greatly differ depending on the Larmor radius. High frequency gyromotion effectively smooths out small fluctuations leading, intuitively, to a lower rate of transport. A reduction in the rate of radial transport with increasing Larmor radius has been shown using the Hasegawa-Mima model [1]. More recently, it was found that, in the limit of large Kubo number, this reduction in transport is less dramatic and in some cases, the rate of transport may increase with the Larmor radius [2]. In [3] it was reported that the zonal flow may strongly influence the rate of transport and the Larmor radius dependence. Here, we investigate these effects using the Hasegawa-Wakatani (HW) model and a modified form which allows the self-generation of zonal flows.

Model equations. The HW equations for density n and the vorticity $\omega = \nabla^2\phi$, where ϕ is the electrostatic potential, are

$$\frac{\partial n}{\partial t} = -\kappa\frac{\partial \phi}{\partial y} + [n,\phi] + \alpha(\phi - n) + \mu\nabla^2 n \;, \; \frac{\partial \omega}{\partial t} = [\omega,\phi] + \alpha(\phi - n) + \mu\nabla^2\omega \;. \qquad (1)$$

In tokamaks, the zonal components of the potential and density do not contribute to the parallel current [4] and in the standard formulation of the equations (1), zonal flows are damped. Modified equations which allow the self-generation of zonal flows, are obtained by subtracting the zonal components from the parallel coupling terms [5],

$$\frac{\partial n}{\partial t} = -\kappa\frac{\partial \phi}{\partial y} + [n,\phi] + \alpha(\tilde{\phi} - \tilde{n}) + \mu\nabla^2 n \;, \; \frac{\partial \omega}{\partial t} = [\omega,\phi] + \alpha(\tilde{\phi} - \tilde{n}) + \mu\nabla^2\omega \;, \qquad (2)$$

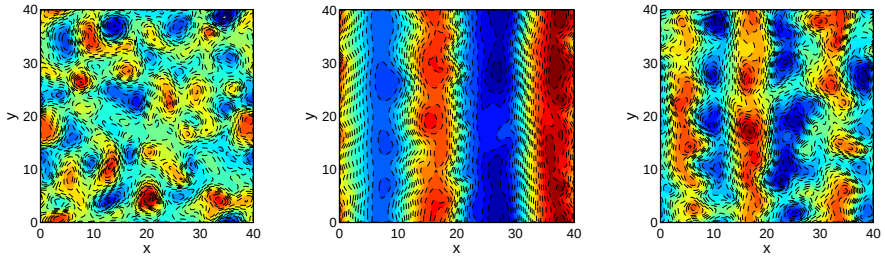

Figure 1: Snapshot of potential ϕ in the saturated quasi-stationary turbulent state for three related models: (left) HW defined by equations 1 where zonal flows are damped; (centre) MHW defined by equations 2 allowing the self-generation of zonal flows; (right) intermediate state of MHW where total kinetic energy of zonal flows is set equal to that of non-zonal drift wave turbulence at each time step.

where $\tilde{\phi} = \phi - \langle\phi\rangle$ and $\tilde{n} = n - \langle n\rangle$ are the non-zonal components and angular brackets denote the zonal components. In 2D the zonal component is the average over the

poloidal y direction, $\langle f \rangle = \frac{1}{L_y}\int f dy$. We refer to (2) as the modified Hasegawa-Wakatani (MHW) equations. We solve equations (1) or (2) on a square of side $L = 40$ using 256×256 grid nodes with periodic boundary conditions. The parameters are set to $\kappa = 1$, $\alpha = 0.5$ and $\mu = 0.01$ in every case.

Saturated turbulent state. Typical snapshots of the potential ϕ in the quasi-stationary saturated turbulent state are shown in figure 1. For the HW model, turbulent vortices dominate. For the MHW model, zonal flows dominate; the four zones visible persist throughout the simulation time. An intermediate state is generated by artificially setting the kinetic energy of the zonal flows equal to the kinetic energy of the non-zonal drift wave turbulence at each time step in the saturated turbulent state of the MHW model,

$$\langle E \rangle_K \equiv \frac{1}{2}\int \left(\frac{\partial \langle \phi \rangle}{\partial x}\right)^2 dV = \frac{1}{2}\int (\nabla \tilde{\phi})^2 dV \equiv \tilde{E}_K \, . \tag{3}$$

We find that zonal flows and turbulent vortices then coexist in a quasi-stationary state; the six visible zones in figure 1 persist throughout the simulation time.

Test particle transport. For each value of Larmor radius ρ, a population of 10 000 test particles is initialised at random once the quasi-stationary turbulent state has been reached. We consider the case where all 10 000 test particles share the same Larmor radius ρ as well as the case where the Larmor radii ρ' are distributed around a most probable value ρ. In the latter case, we choose a discrete approximation to the Boltzmann distribution. These two models are equivalent when $\rho = 0$. Provided that the frequency of the gyro-motion is much faster than the frequency of the turbulence, FLR effects can be included [1] simply by spreading the particle over a ring of (Larmor) radius ρ centred on the particle's guiding centre. This is implemented numerically by averaging over N_{gyro} (= 16 in this case) points. Each test

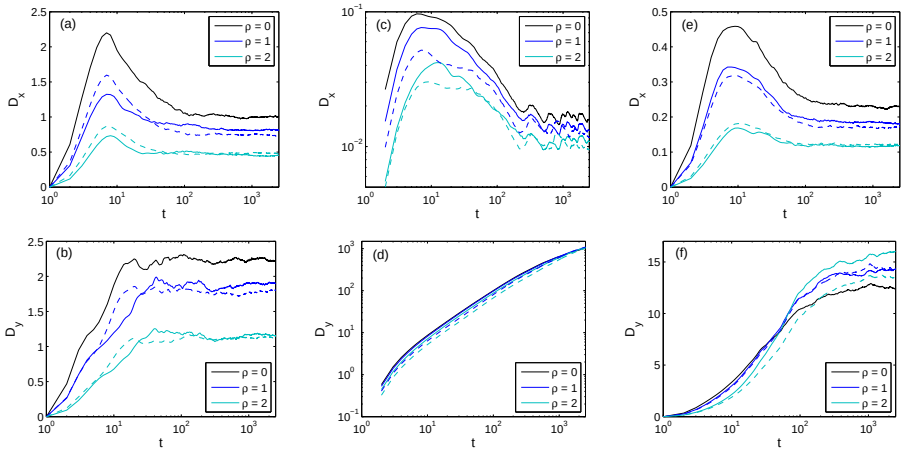

Figure 2: Running diffusion coefficients D_x and D_y versus time: (a) and (b) HW case on a log-linear scale; (c) and (d) MHW case on a log-log scale; (e) and (f) intermediate turbulence case on a log-linear scale. The value of ρ is indicated by the colour of the plotted lines. Full lines indicate results when all the test particle share the same Larmor radius ρ; dashed lines indicate results when the Larmor radii are distributed around a most probable value ρ.

particle has the equation of motion $\partial \mathbf{r}/\partial t = \hat{\mathbf{v}}_E$, where $\hat{\mathbf{v}}_E$ is the gyro-averaged $E \times B$ velocity, $\mathbf{v}_E = (-\partial\phi/\partial y, \partial\phi/\partial x)$. We calculate running diffusion coefficients in the radial x and poloidal y directions separately, $D_x(t) = X(t)^2/2t$, $D_y(t) = Y(t)^2/2t$. Here $X(t)^2 = \langle [x(t) - \langle x(t) \rangle]^2 \rangle$, $Y(t)^2 = \langle [y(t) - \langle y(t) \rangle]^2 \rangle$ and $(x(t), y(t))$ is the position of the particle with respect to its initial position; angular brackets denote an ensemble average over the 10 000 test particles. For a 'normal' diffusive process the running diffusion coefficient will reach a value independent of time since $X(t)^2 \sim t$. More generally the transport may be 'anomalous' and $X(t)^2 \sim t^\sigma$, where $0 < \sigma < 1$ implies subdiffusion and $1 < \sigma < 2$ implies superdiffusion. In figure 2 we plot $D_x(t)$ and $D_y(t)$ for $\rho = [0, 1, 2]$ for all the cases considered.

Figures 2 (a) and (b) show the results for the HW case. For all cases the running diffusion coefficients converge on time independent values, indicating normal diffusive processes. Figures 2 (c) and (d) show the results for the MHW case on a log-log scale. We find that the running diffusion coefficients are not time independent. Poloidal diffusion (along the zones) is superdiffusive with exponent $\sigma \approx 1.7$ and radial diffusion (across the zones) is subdiffusive with $\sigma \approx 0.8$. We note that zonal flows drastically reduce radial transport, while the poloidal transport is orders of magnitude larger than the HW case. Figures 2 (e) and (f) show the results for the intermediate turbulence case. The running diffusion coefficients converge on time independent values, indicating normal diffusive processes.

Larmor radius dependence. In figure 3 we plot the values of D_x and D_y at the end of the simulation ($t = 2500$) as a function of ρ for all the cases considered. It should be noted that the results for the MHW case do not represent true diffusion coefficients since D_x and D_y change with time and the figures are plotted for comparison purposes. Figures 2 (a) and (b) show the results for the HW case. For all cases, the diffusion coefficients decrease as ρ increases. A transition between regions of faster and slower

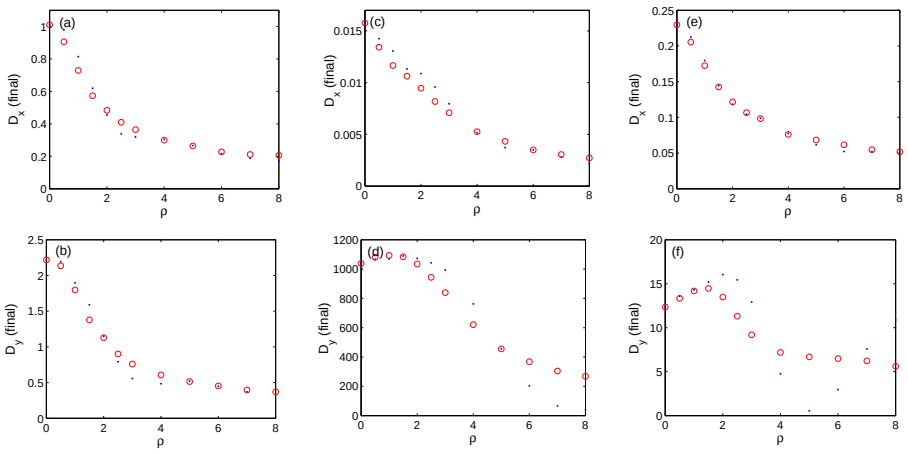

Figure 3: Value of diffusion coefficients D_x and D_y at the end of the simulation ($t = 2500$) as a function of ρ: (a) and (b) HW case; (c) and (d) MHW case; (e) and (f) intermediate turbulence case. Blue dots indicate results when all the test particle share the same Larmor radius ρ; red circles indicate results when the Larmor radii are distributed around a most probable value ρ.

decline occurs around $\rho = 3$ which equates to the typical radius of the turbulent vortices seen in snapshots of the potential (figure 1). Figures 2 (c) and (d) show the results for the MHW case. The Larmor radius dependence of the poloidal diffusion coefficient D_y is radically different from the HW case. For small values of ρ, D_y increases with ρ. For larger ρ, the rate at which D_x and D_y decline with increasing ρ is smaller than in the HW case. For large values of ρ, the Larmor radius dependence of D_y significantly differs between the case where all test particles share the same ρ and the case where the Larmor radii follow a distribution. In the former case, D_y falls off almost to zero at $\rho = 8$ which corresponds to the radial half-wavelength of the zonal flow, so that the effects of the zonal flow are maximally averaged out. Figures 2 (e) and (f) show the results for the intermediate turbulence case. The Larmor radius dependence has similarities to the MHW case. The radial diffusion coefficient D_x decreases with ρ. For small ρ, the poloidal diffusion coefficient D_y increases with ρ, and this effect is larger than in the MHW case. For larger ρ, when all the test particles share the same Larmor radius, D_y decreases to a minimum around $\rho = 5$ and this corresponds to the radial half-wavelength of the zonal flow. The value of D_y at this minimum is very close to the corresponding value for the HW case. When the test particles have a distribution of Larmor radii, there is no such minimum, and D_y falls off slowly with large ρ.

Discussion. With zonal flows present, when all test particles share the same Larmor radius, D_y falls off with ρ to a minimum which corresponds to the half-wavelength of the zonal flow. This minimum might be expected since test particles with ρ equal to the half-wavelength of the zonal flow will sample one full period of the zonal potential, leading to a low rate of poloidal transport since the sum over one period should be close to zero. No such minimum occurs when the test particles have a distribution because a significant fraction of the test particles will have Larmor radii not equal to the zonal flow half-wavelength. Intuitively, increasing the Larmor radius ρ should lead to a decrease in diffusion since increasingly large fluctuations are averaged out. In the HW case, we observe this decrease. However, when zonal flows and turbulent vortices coexist (as in the MHW and intermediate cases) we find that the poloidal diffusion D_y increases with ρ for small ρ. This may be explained by the fact that increasing ρ also decreases the amount of trapping due to turbulent vortices. When ρ is small, test particles can be trapped in vortices and effectively shielded from the zonal flow. As ρ is increased the amount of trapping is reduced, so that the test particles are more exposed to the zonal flow potential, leading to an increase in D_y. This effect is stronger in the intermediate case than in the MHW case, due to the presence of larger turbulent vortices. No increase in D_x is observed, because zonal flows do not produce radial diffusion.

Acknowledgements. This work was supported in part by the EPSRC and by Euratom. JMD acknowledges support from an EPSRC CASE studentship in association with UKAEA. The content of the publication is the sole responsibility of the authors and it does not necessarily represent the views of the Commission of the European Union or their services.

References

[1] Manfredi G and Dendy R O 1996 *Phys. Rev. Lett.* **76** 4360
[2] Vlad M and Spineanu F 2005 *Plasma Phys. Control. Fusion* **47** 281
[3] Hauff T and Jenko F 2007 *Phys. Plasmas* **14** 92301
[4] Dorland W and Hammett G W 1993 *Phys. Fluids B* **5** 812
[5] Numata R, Ball R and Dewar R L 2007 *Phys. Plasmas* **14** 102312